JACS
JOURNAL OF THE AMERICAN CHEMICAL SOCIETY

Folding of Oligoviologens Induced by Radical-Radical Interactions

Yuping Wang,[†] Marco Frasconi,[†] Wei-Guang Liu,[‡] Zhichang Liu,[†] Amy A. Sarjeant,[†] Majed S. Nassar,[§] Youssry Y. Botros, [§,⊥] William A. Goddard III,[‡] and J. Fraser Stoddart*[,†]

[†]*Department of Chemistry, Northwestern University, 2145 Sheridan Road, Evanston, Illinois 60208, USA*

[‡]*Materials and Process Simulation Center, California Institute of Technology, 1200 East California Boulevard, Pasadena, California 91125, USA*

[§]*Joint Center of Excellence in Integrated Nano-Systems (JCIN), King Abdul-Aziz City for Science and Technology (KACST), P.O. Box 6086, Riyadh 11442, KSA*

[⊥]*University Research Office, Intel Corporation, Building RNB-6-61, 2200 Mission College Boulevard, Santa Clara, California 95054, USA*

*E-mail: stoddart@northwestern.edu

Supporting Information

Table of Contents

1. Materials and General Methods

Chemicals were purchased as reagent grade and employed without further purification. Commercial grades of anhydrous MeCN and *N*,*N*-dimethylformamide (DMF) were used as solvents in all reactions. Compounds **5V**•10PF_6, in addition to the precursors **S1**•2PF_6 and **S3**•2PF_6, were prepared according to literature procedures.[1] Thin layer chromatography (TLC) was performed on silica gel 60F254 (E Merck). Column chromatography was carried out on silica gel 60F (Merck 9385, 0.040–0.063 mm). High performance liquid chromatography (HPLC) was performed on a preparative RP-HPLC instrument, using a C_{18} column (Agilent, 10μm packing, 30 mm × 250 mm). The eluents employed were MeCN and H_2O, both mixed with 0.1 % (v/v) trifluoroacetic acid (TFA). The detector was set to λ = 254 nm. HPLC Analysis was performed on an analytical RP-HPLC instrument, using a C_{18} column. For UV/Vis/Near Infrared (NIR) studies, all sample preparations were performed in an Argon-filled atmosphere. Samples were loaded into quartz 1 cm tubes and sealed and used immediately after preparation. Nuclear magnetic resonance (NMR) spectra were recorded at 298 K on Bruker Avance 500 and 600 spectrometers, with working frequencies of 500 and 600 MHz for ^{1}H, and 125 and 150 MHz for ^{13}C nuclei, respectively. Chemical shifts are reported in ppm relative to the signals corresponding to the residual non-deuterated solvents.[2] High-resolution mass spectra were measured on an Agilent 6210 Time-of-Flight (TOF) LC-MS, using an ESI source, coupled with Agilent 1100 HPLC stack, using direct infusion (0.6 mL min^{-1} Measurements at X-band (9.5 GHz) were performed with a Bruker Elexsys E580, equipped with a variable Q dielectric resonator (ER-4118X-MD5-W1). Cyclic voltammetry experiments were performed on a Princeton Applied Research 263 A Multipurpose instrument interfaced to a PC, using a glassy carbon working electrode (0.071 cm^2, Cypress system). The electrode surface was polished routinely with an

alumina/water slurry on a felt surface immediately before use. The counter electrode was a Pt coil and the reference electrode was an AgCl coated Ag wire. The concentrations of the samples were 1 mM in 100 mM electrolyte solutions of tetrabutyl- ammonium hexafluorophosphate ($TBAPF_6$) in MeCN.

2. Synthetic Protocols

Scheme S1. One-step synthesis of S2•4PF$_6$ from S1•2PF$_6$

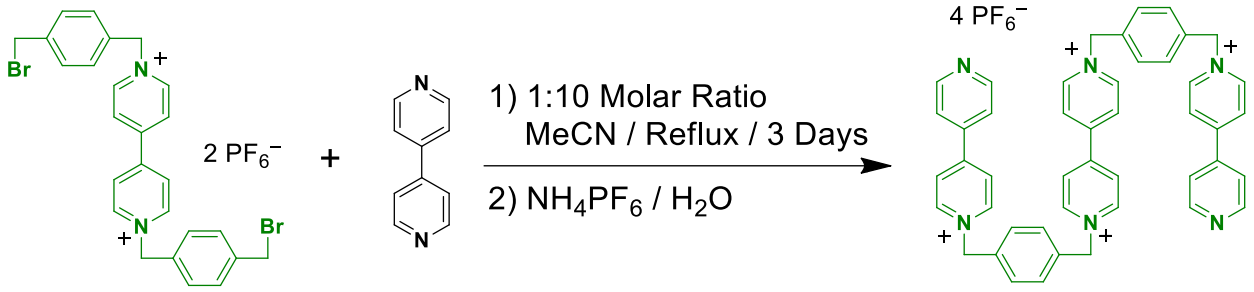

S1•2PF$_6$ **S2**•4PF$_6$

S2•4PF$_6$: A solution of 4,4′-bipyridine (1.56 g, 10 mmol) in MeCN (40 mL) was added dropwise via syringe at 4 mL / h to a refluxing solution of **S1**•2PF$_6$ (814 mg, 1 mmol) in MeCN (40 mL) at 80 ℃. After addition, the reaction mixture was stirred for a further 72 h under reflux, and then cooled to room temperature. The yellow precipitate was filtered off and washed with Me_2CO, Et_2O, and finally purified by column chromatography (SiO_2) using 2 % NH_4PF_6 (m/v) Me_2CO solution as the eluent. The fractions were monitored by mass spectrometry and analytical HPLC. The pure fractions were combined, concentrated under vacuum, reprecipitated in H_2O, filtered off and washed with H_2O, MeOH and finally Et_2O to afford **S2**•4PF$_6$ as a white crystalline solid (1.01 g, 80 %). ^{1}H NMR (500 MHz, CD_3CN): δ = 8.97 (d, *J* = 5.0 Hz, 4H), 8.92 (m, 8H), 8.97 (d, *J* = 5.0 Hz, 4H), 8.41 (m, 8H), 8.09 (d, *J* = 5.0 Hz, 4H), 7.60 (s, 8H), 5.87 (s, 4H), 5.87 (s, 4H). ^{13}C NMR (126 MHz, CD_3CN): δ = 145.4, 134.2, 133.9, 130.0, 130.0, 129.9, 127.2, 126.8, 124.5, 63.6, 63.4. HRMS (ESI): *m/z* calcd for $C_{46}H_{40}F_{18}N_6P_3$ $[M - PF_6]^+$ 1111.2233, found 1111.2234

Scheme S2. Methylation of S2•4PF$_6$ to give 3V•6PF$_6$

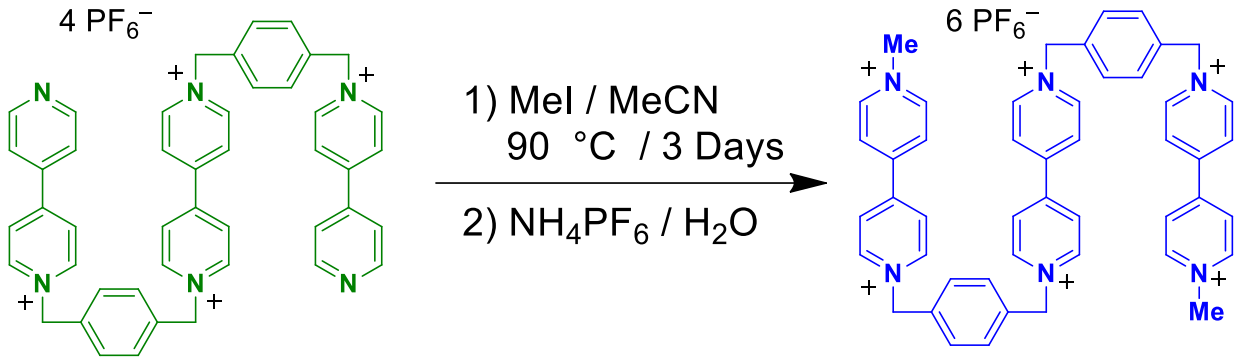

S2•4PF$_6$ **3V**•6PF$_6$

3V•6PF$_6$: MeI (251 mg, 1.85 mmol) was added dropwise to a solution of **S2**•4PF$_6$ (125 mg, 0.1 mmol) in DMF (3 mL) with stirring at room temperature. After addition, the mixture was then heated to 90 ℃ for 72 h. The reaction mixture was cooled to room temperature. When Me_2CO was added to the solution, white precipitates formed immediately. The resulting precipitate was filtered off, washed with Me_2CO and re-dissolved in H_2O. An excess of NH_4PF_6 was added to this solution until no further precipitation was observed. The crude product was filtered off, washed sequentially with H_2O, MeOH, and finally Et_2O, dried under vacuum to afford **3V**•6PF$_6$ as a white solid (142 mg, 90 %). ^{1}H NMR (500 MHz, CD_3CN): δ = 8.98 (d, *J* = 5.0 Hz, 8H), 8.87 (d, *J* = 5.0 Hz, 4H), 8.41 (m, 8H), 8.38 (d, *J* = 5.0 Hz, 4H), 7.61 (s, 8H), 5.87 (s, 8H), 4.42 (s, 6H). ^{13}C NMR (126 MHz, CD_3CN): δ = 150.1, 145.3, 144.1, 134.0, 134.0, 130.0, 130.0, 129.9, 127.2, 127.2, 127.1, 126.5, 125.4, 63.6. HRMS (ESI): *m/z* calcd for $C_{48}H_{46}F_{30}N_6P_5$ [*M* – PF_6]$^+$ 1431.1988, found 1431.1982.

Scheme S3. One-step synthesis of S4•6PF$_6$ and S5•22PF$_6$ from S3•6PF$_6$

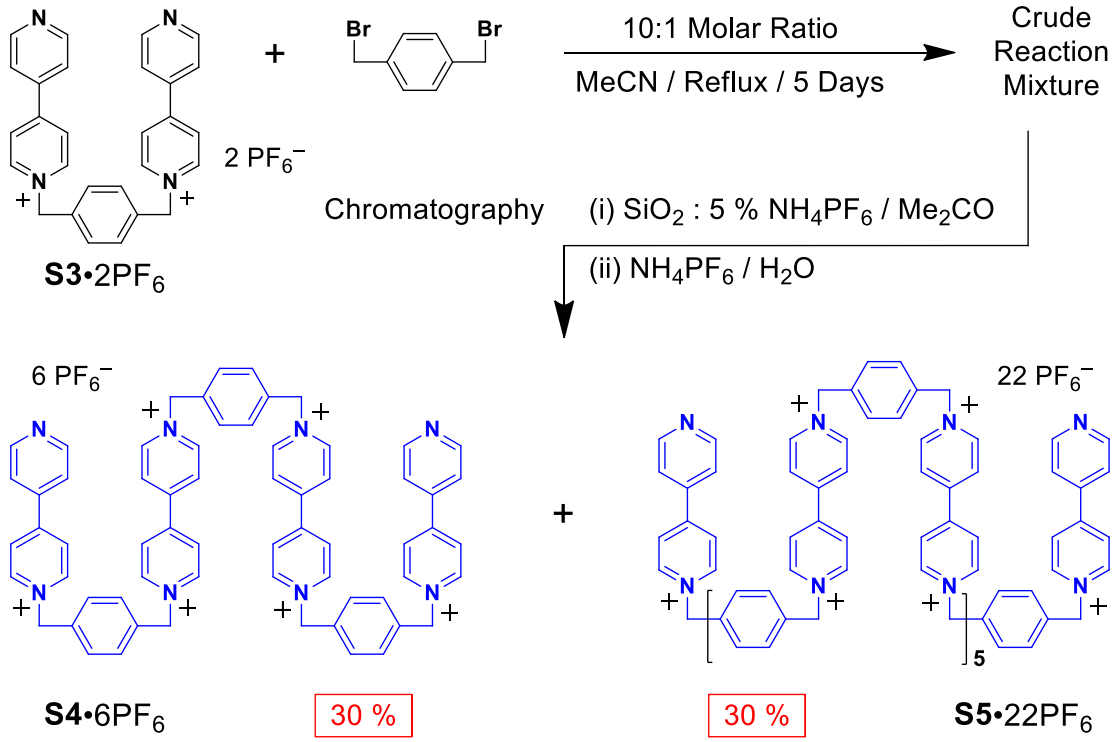

S4•6PF$_6$ / **S5•22PF$_6$**: A solution of 1,4-bis(bromomethy1)benzene (1.1 g, 4.1 mmol) in dry MeCN (40 mL) was added over 10 h to a solution of **S3**•2PF$_6$ (6.25 g, 40 mmol) in dry MeCN (50 mL) while being heated under reflux. The mixture was heated for a further 120 h after the addition, and then cooled to room temperature. The yellow precipitate was filtered off and washed with Me_2CO, Et_2O, and finally purified by column chromatography (SiO_2) using 5 % NH_4PF_6 (m/v) Me_2CO solution as the eluent. The fractions were monitored by mass spectrometry and analytical HPLC. The pure fractions were combined, concentrated under vacuum, reprecipitated in H_2O, filtered off and washed with H_2O (50 mL), MeOH (20 mL) and finally Et_2O (50 mL) to afford **S4**•4PF$_6$ (2.22 g, 30 %) and **S5**•22PF$_6$ (1.52 g, 30 %) as white crystalline solids. **S4**•4PF$_6$: ^{1}H NMR (500 MHz, CD_3CN): δ = 8.97 (d, *J* = 5.0 Hz, 8H), 8.87 (m, 8H), 8.41 (d, *J* = 5.0 Hz, 8H), 8.36 (d, *J* = 5.0 Hz, 4H), 7.82 (d, *J* = 5.0 Hz, 4H), 7.61 (s, 4H), 7.60 (s, 8H), 5.87 (s, 8H), 5.81 (s, 4H). ^{13}C NMR (126 MHz, CD_3CN): δ = 154.3, 150.7, 150.1, 145.3, 144.7, 140.9, 134.4, 134.0, 133.8, 130.0, 130.0, 129.8, 127.2, 126.0, 121.6, 117.0, 63.7, 63.6, 63.0.

HRMS (ESI): *m/z* calcd for $C_{64}H_{56}F_{30}N_8P_5$ $[M - PF_6]^+$ 1661.2831, found 1661.2811. **S5**•22PF_6: ^{1}H NMR (500 MHz, CD_3CN): δ = 8.97 (d, *J* = 5.0 Hz, 40H), 8.87 (m, 8H), 8.41 (d, *J* = 5.0 Hz, 40H), 8.37 (d, *J* = 5.0 Hz, 4H), 7.95 (d, *J* = 5.0 Hz, 4H), 7.61 (m, 44H), 5.87 (s, 40H), 5.81 (s, 4H). ^{13}C NMR (126 MHz, CD_3CN): δ = 150.1, 145.3, 134.0, 130.0, 129.9, 129.8, 127.2, 126.3, 63.6. HRMS (ESI): *m/z* calcd for $C_{208}H_{184}N_{24}F_{114}P_{19}$ $[M - 3PF_6]^{3+}$ 1924.2796, found 1924.2642.

Scheme S4. Methylation of S4•6PF_6 to give 4V•8PF_6

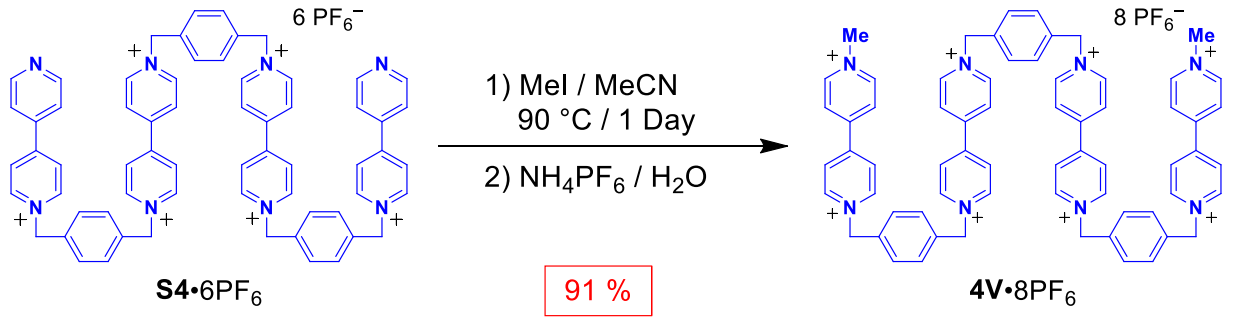

4V•8PF_6: MeI (251 mg, 1.85 mmol) was added dropwise to a solution of **S4**•6PF_6 (181 mg, 0.1 mmol) in DMF (3 mL) with stirring at room temperature. After addition, the mixture was then heated to 90 ℃ for 72 h and cooled to room temperature, and then Me_2CO was added to the solution. The resulting precipitate was filtered off, washed with Me_2CO, re-dissolved in H_2O, and re-precipitated by adding an excess of NH_4PF_6. The solid was filtered off and washed with H_2O, MeOH and finally Et_2O to afford **4V**•8PF_6 as a white solid (196 mg, 92 %). ^{1}H NMR (500 MHz, CD_3CN): δ = 8.98 (d, *J* = 5.0 Hz, 12H), 8.87 (d, *J* = 5.0 Hz, 4H), 8.41 (m, 12H), 8.38 (d, *J* = 5.0 Hz, 4H), 7.61 (s, 12H), 5.87 (s, 12H), 4.42 (s, 6H). ^{13}C NMR (126 MHz, CD_3CN): δ = 150.2, 149.1, 146.1, 145.3, 134.0, 130.0, 130.0, 127.2, 127.2, 126.5, 63.6. For crystal growing experiments, **4V**•8PF_6 was converted to **4V**•8SbF_6: **4V**•8PF_6 was dissolved in MeCN and precipitated by adding an excess of TBACl. The solid was filtered off and washed with Me_2CO, then re-dissolved in H_2O and re-precipitated by adding an excess of $KSbF_6$ to afford **4V**•8SbF_6 as a white solid. HRMS (ESI): *m/z* calcd for $C_{66}H_{62}F_{36}N_8Sb_6$ $[M - 2SbF_6]^{2+}$ 1189.9379, found 1189.9381.

Scheme S5. Methylation of S5•22PF$_6$ to give 12V•24PF$_6$

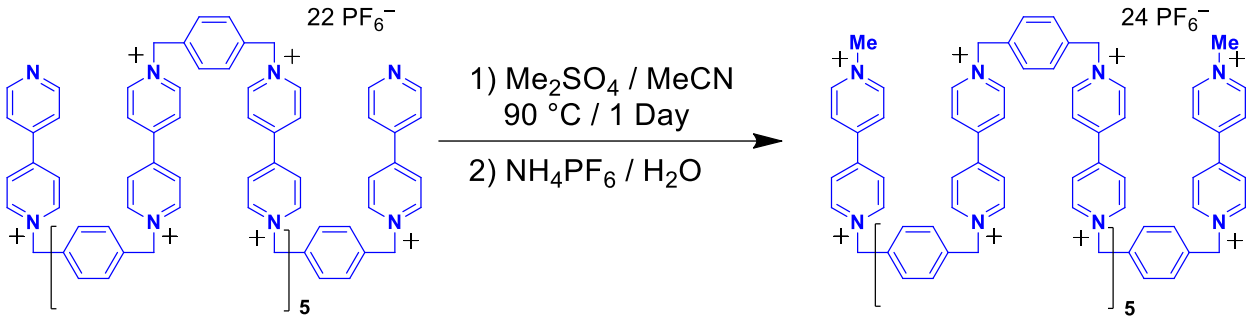

S5•22PF$_6$ 90 % **12V**•24PF$_6$

12V•24PF$_6$: Dimethyl sulfate (300 mg, 2.38 mmol) was added to a solution of **S5**•22PF$_6$ (100 mg, 0.016 mmol) in DMF (3 mL). The mixture was heated to 90 ℃ for 5 days and cooled to room temperature and then Me_2CO was added to the solution. The resulting precipitate was filtered off, washed with Me_2CO and re-dissolved in H_2O, and re-precipitated by adding an excess of NH_4PF_6. The solid was filtered off and washed with H_2O, MeOH and finally Et_2O to afford **12V**•24PF$_6$ as a white solid (102 mg, 98 %). ^{1}H NMR (500 MHz, CD_3CN): δ = 8.98 (d, *J* = 5.0 Hz, 44H), 8.87 (d, *J* = 5.0 Hz, 4H), 8.42 (d, *J* = 5.0 Hz, 44H), 8.38 (d, *J* = 5.0 Hz, 4H), 7.62 (s, 44H), 5.87 (s, 44H), 4.42 (s, 6H). ^{13}C NMR (126 MHz, CD_3CN): δ = 151.1, 146.3, 134.9, 130.9, 130.9, 128.2, 128.1, 127.4, 64.6, 30.5. HRMS (ESI): *m/z* calcd for $C_{210}H_{190}N_{24}F_{126}P_{21}$ [*M* – 3PF$_6$]$^{3+}$ 2030.9371, found 2030.9343.

The ^{1}H NMR spectra of these five oligoviologens show a similar set of six peaks, corresponding to the protons of (i) the BIPY^{2+}units, (ii) the phenylene rings, (iii) the methylene groups and (iv) terminal methyl substituents. The ratio of H_α to H_α', as well as H_β to H_β' increases as the oligoviologen becomes longer (Figure S1).

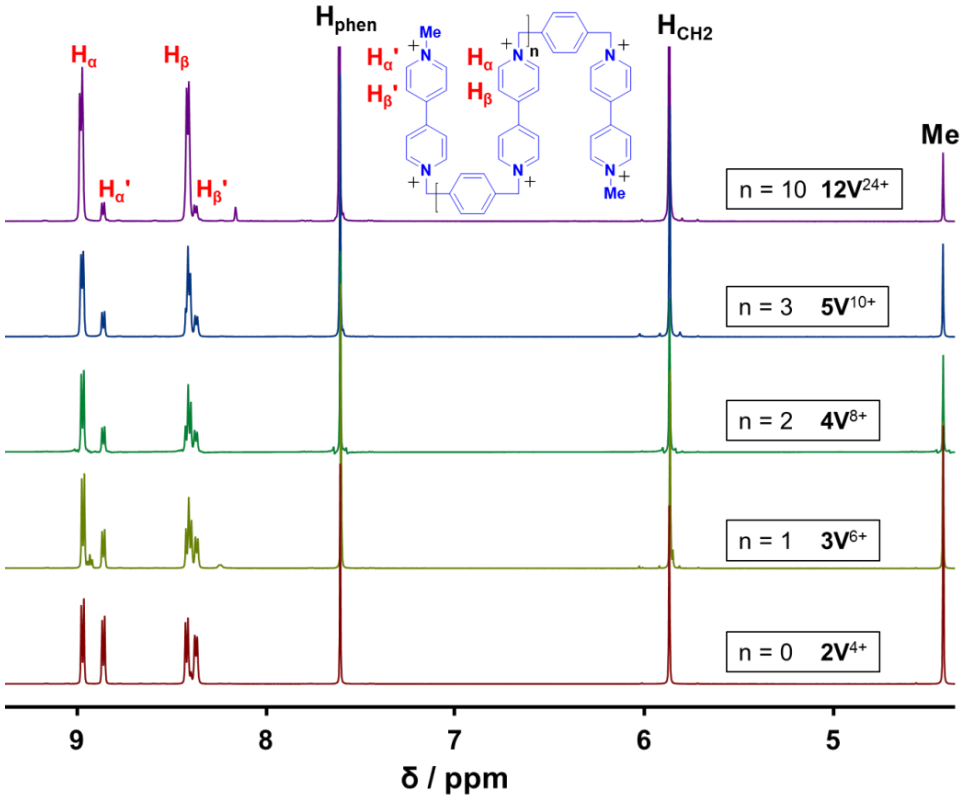

Figure S1. ^{1}H NMR Spectra (500 MHZ, CD_3CN, 298K) of oligoviologens **2V**$^{4+}$ to **12V**$^{24+}$.

Moreover, the environment of the protons on the phenylene rings and methylene groups show no anisochronous behavior and so as a result they both appear as an apparent singlet. It is also noteworthy that from **2V**$^{4+}$ all the way up to **12V**$^{24+}$, the increment of BIPY^{2+} subunits further lowers the electron density around BIPY^{2+} protons, leading to a 0.01 ppm downfield shift of H_{α}.

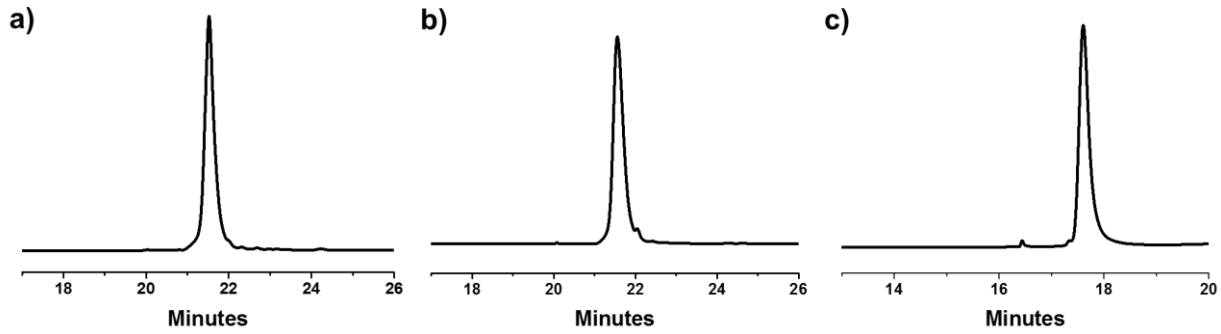

Figure S2. Analytical RP-HPLC chromatograms (H_2O–MeCN, 0.1% TFA, 0–100% MeCN in 60 min, λ = 254 nm) of **3V**$^{6+}$, **4V**$^{8+}$ and **12V**$^{24+}$. The highest charged compound **12V**$^{24+}$ has the shortest retention time on the column.

3. UV / Vis Absorption Spectroscopy

When one considers all the UV/Vis/NIR spectra for the oligoviologens together, the shifts in the wavelengths of the absorption bands, a phenomenon which reflects their folding modes in solution, are not unexpected taking into account the following facts — (i) the $BIPY^{\bullet+}$ radical cationic subunits have a marked tendency to form a complex as a result of the radical-radical interactions in solution, with the larger the number of $BIPY^{\bullet+}$ subunits corresponding to increased complex stability, and (ii) the $BIPY^{\bullet+}$ radical cationic subunits can interact with each other either intra- or intermolecularly, respectively, depending upon (a) the flexibility of the oligoviologens and (b) the entropy penalty paid when bringing two oligoviologens together.

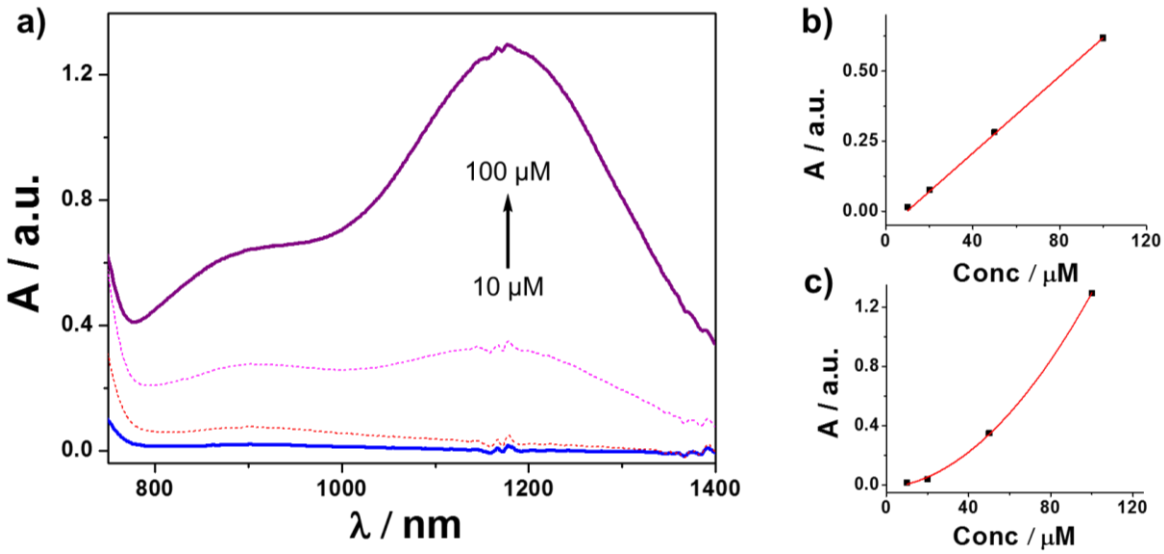

Figure S3. **a)** Partial UV/Vis/NIR spectra of the absorption bands of $\mathbf{4V}^{4(\bullet+)}$ recorded over a range of concentrations from 10 to 100 µM. **b)** The intensity of the absorption band at 900 nm varies linearly with concentration, confirming that this absorption can be attributed to intramolecular interactions. **c)** The intensity of the absorption band at 1177 nm varies non-linearly with concentration, confirming that this absorption can be attributed to intermolecular interactions.

The longest homologue, namely $\mathbf{12V}^{12(\bullet+)}$, has enough flexibility to form an intramolecular complex involving multiple $BIPY^{\bullet+}$ subunits which give rise (Figure 2b) to the most red-shifted absorption band at 1320 nm. As the oligoviologen homologues become shorter, as in the cases of $\mathbf{4V}^{4(\bullet+)}$ and $\mathbf{5V}^{5(\bullet+)}$, only an intramolecular $BIPY^{\bullet+}$ dimer can form on account of their limited

conformational freedom, giving rise (Figure 2a) to an absorption band at 900 nm which is 420 nm blue-shifted. In addition, $BIPY^{\bullet+}$ subunits interact intermolecularly, affording an absorption band above 1100 nm. In the cases of $\mathbf{2V}^{2(\bullet+)}$ and $\mathbf{3V}^{3(\bullet+)}$, however, their short and rigid structural features mitigate against the formation of intramolecular complexes, and instead, intermolecular radical-radical interactions-driven complexes are formed.

Based on this hypothesis, it is evident from the perspective of the flexibility of oligoviologens that, while $\mathbf{4V}^{4(\bullet+)}$ shows (Figure S3) similar spectroscopic features to $\mathbf{5V}^{5(\bullet+)}$ (Figure S4), i.e., two absorption bands in the NIR region with one centered on 900 and the other above 1100 nm, the absorption intensity ratio of the two absorption bands — corresponding to their ability to become involved in intra-molecular complexation — is lower (compare Figure S3 and S4) in the case of $\mathbf{4V}^{4(\bullet+)}$.

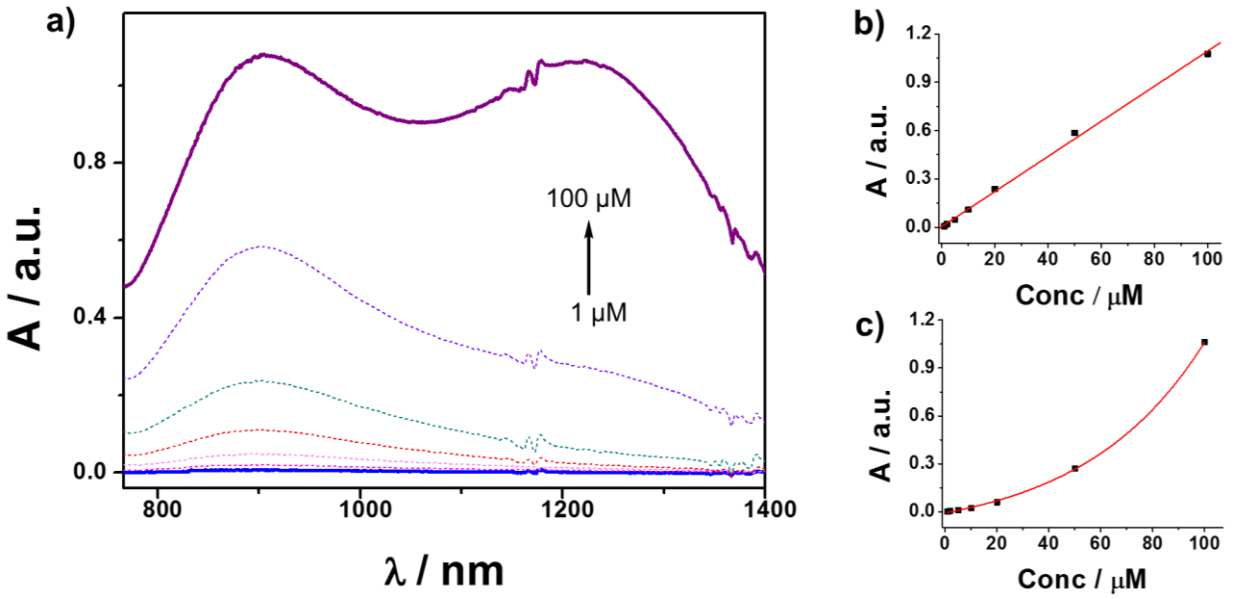

Figure S4. **a)** Partial UV/Vis/NIR spectra of the absorption bands of $\mathbf{5V}^{5(\bullet+)}$ recorded over a range of concentrations from 1 to 100 µM. **b)** The intensity of the absorption band at 900 nm varies linearly with concentration, confirming that this absorption can be attributed to intramolecular interactions. **c)** The intensity of the absorption band at 1225 nm varies non-linearly with concentration, confirming that this absorption is concentration dependent and can be attributed to intermolecular interactions. The absorption spectra also indicate that, while both types of interactions contribute to controlling the folding properties at relatively high concentrations (100 µM), intramolecular interactions dominate the folding behavior at relatively low concentration (25 µM).

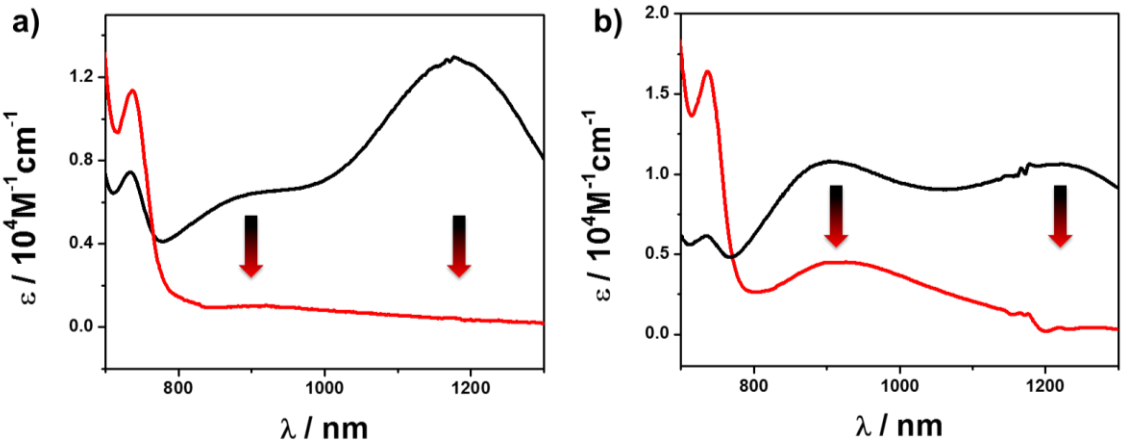

Figure S5. a) Partial UV/Vis/NIR absorption spectra of **4V**$^{4(\bullet+)}$ recorded in MeCN (black) and MeCN / DMF (3:7, v/v) (red) at a concentration of 1×10^{-4} M at 298 K. **b)** Partial UV/Vis absorption spectra of **5V**$^{5(\bullet+)}$ recorded in MeCN (black) and MeCN / DMF (3:7, v/v) (red) at a concentration of 0.1 mM at 298 K. As a result of lower radical-radical interaction strengths between BIPY$^{\bullet+}$ subunits in DMF, the absorption bands centered on 900 and 1177 nm for **4V**$^{4(\bullet+)}$, as well as those centered on 900 and 1225 nm for **5V**$^{5(\bullet+)}$, decrease in their intensities in the mixed solvent. The more significant decreases in absorption at 1177 and 1225 nm, compared with that at 900 nm, points to their intermolecular interactional properties.

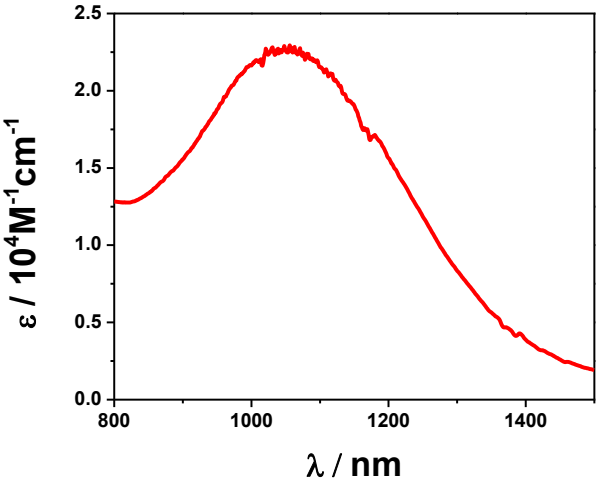

Figure S6. Partial UV/Vis absorption spectra of **2V**$^{2(\bullet+)}$ recorded in MeCN at 298 K at a concentration of 1 mM. The absorption band at 1050 nm indicates the existence of intermolecular radical-radical interactions between BIPY$^{(\bullet+)}$ subunits in solution.

More evidence for the assignment of the intramolecular and intermolecular absorption bands can be obtained (Figure S5) by performing UV/Vis/NIR measurements in a mixed solvent system of MeCN /DMF (3:7, v/v), given the fact that the binding strength between BIPY$^{\bullet+}$ units is much lower in DMF than that in MeCN. As a result, the absorption bands, which correspond

to intermolecular interactions, experience a much larger decrease in intensity in DMF compared with their intramolecular counterparts. In fact, the absorption bands above 1100 nm decrease more significantly than the bands around 900 nm in the cases of both $\mathbf{4V}^{4(\bullet+)}$ and $\mathbf{5V}^{5(\bullet+)}$, an observation which is in good agreement with our original hypothesis.

In the case of $\mathbf{12V}^{12(\bullet+)}$, what is yet more noteworthy is the fact that no absorption band is observed in the region around 1100 nm, even at concentrations as high as 100 μM. This observation confirms the lack of intermolecular interactions between $\mathbf{12V}^{12(\bullet+)}$, a situation which can be ascribed to the entropic penalty that would be paid by implicating intermolecular interactions, hence disfavoring this binding process.

4. X-Ray Crystallography

Crystallization Procedure: A 0.2 mM MeCN solution of $\mathbf{3V}\bullet 6PF_6$ was reduced by Zn dust to generate $\mathbf{3V}^{3(\bullet+)}$ before being filtered through a Pall syringe filter (pore size 0.45 μm) into VWR culture tubes (6 × 50 mm). The tubes were allowed to stand at room temperature in a closed scintillation vial containing iPr$_2$O (3 mL). After two weeks, purple crystals of $[\mathbf{3V}^{3(\bullet+)}]_2\bullet 6PF_6$ appeared in the tubes from which a rod-like crystal was picked out and mounted using oil (Infineum V8512) on a glass fiber and transferred to the cold gas stream, cooled by liquid N_2 on a Bruker APEX-II CCD with graphite monochromated Mo-Kα radiation. The superstructure was solved by direct methods and refined subsequently using the OLEX2 software.[2]

Crystal data for $[\mathbf{3V}^{3(\bullet+)}]_2\bullet 6PF_6$: $C_{96}H_{92}F_{36}N_{12}P_6$, M = 2283.63, crystal size 0.175 × 0.085 × 0.077 mm^3, orthorhombic, space group *Pnma*, a = 25.5439(8), b = 26.3802(8), c = 38.3250(13) Å, $\alpha = \beta = \gamma = 90$ °, V = 25825.4(1) Å^3, T = 100(2) K, Z = 6, ρ_{calc} = 1.175. Of a total of 119860 reflections that were collected ($4.066 \leq 2\Theta \leq 130.284$), 22396 were unique ($R_{int}$ = 0.0559, R_{sigma} = 0.0396). Final R_1 $(F^2 > 2\sigma F^2)$ = 0.1047, wR_2 = 0.3022. Data were collected at 100 K using a Bruker d8-APEX II CCD diffractometer (CuKα radiation, λ = 1.54178 Å). Intensity data were collected using ω and φ scans spanning at least a hemisphere of reciprocal space for all structures (data were integrated using SAINT). Absorption effects were corrected on the basis of multiple

equivalent reflections (SADABS). The superstructure was solved by direct methods (SHELXS) and refined by full-matrix least-squares against F_2 (SHELXL). The crystal data for $[\mathbf{3V}^{3(\bullet+)}]_2 \bullet 6PF_6$ contained diffuse, disordered solvent molecules and PF_6^- counterions that could not be adequately modeled.

5. Computational Study of the Folding Process of the Oligoviologens

In solution, the folded superstructures of the oligoviologens can be controlled by either intra- or intermolecular interactions, depending on their concentrations and the lengths of the molecules. We used the M06-L flavor of DFT as described in the computational details section to optimize the folded superstructures of the four oligoviologens from $\mathbf{2V}^{2(\bullet+)}$ to $\mathbf{5V}^{5(\bullet+)}$ for both intra- and intermolecular binding modes. We find that, for the intermolecular binding mode, all four oligoviologens show a considerable tendency to form a homodimer as a result of intercalating with each other, courtesy of radical-radical interactions (Figure S7).

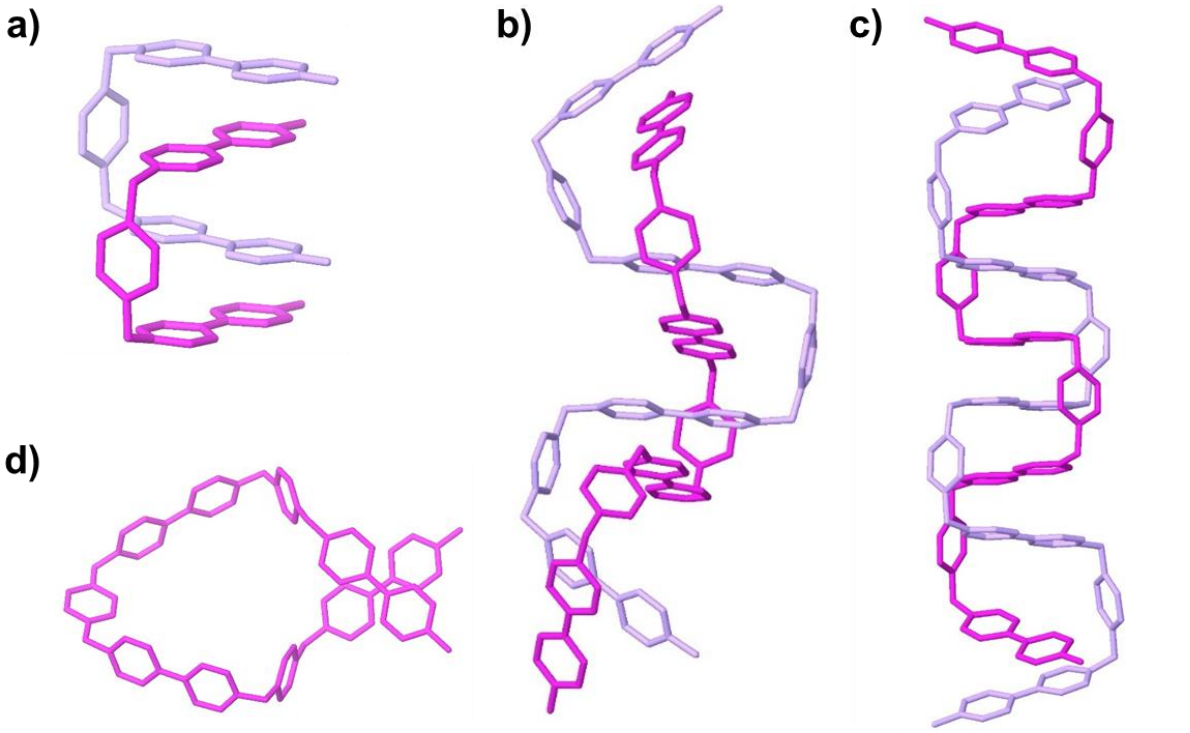

Figure S7. DFT predicted superstructures of the homodimer of **a)** $\mathbf{2V}^{2(\bullet+)}$, **b)** $\mathbf{4V}^{4(\bullet+)}$ and **c)** $\mathbf{5V}^{5(\bullet+)}$ for intermolecular binding mode, indicating the formation of an intercalated dimer is preferred. **d)** DFT predicted conformations of $\mathbf{4V}^{4(\bullet+)}$ in the intramolecular binding mode, indicating that two $BIPY^{(\bullet+)}$ subunits at each end of the chain can interact with each other.

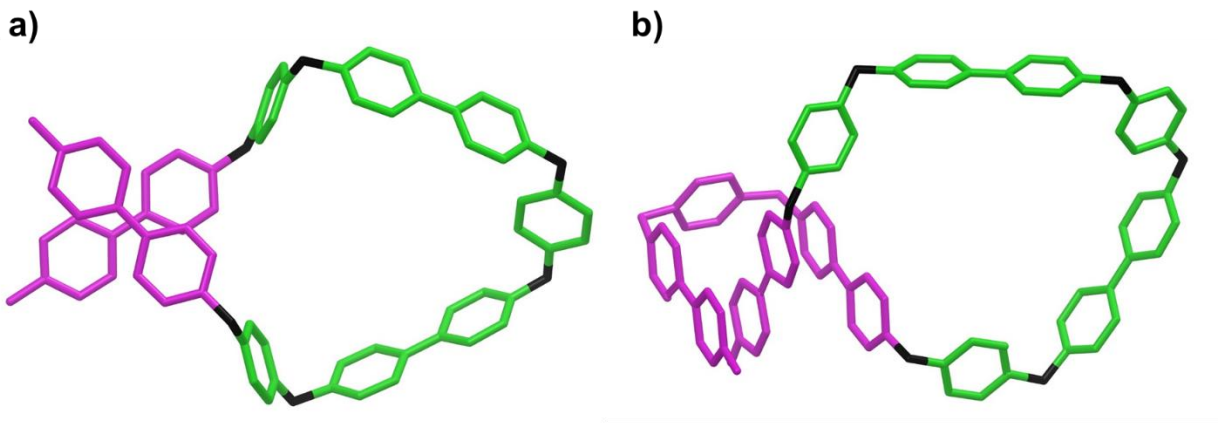

Figure S8. The rotatable fragments in the intramolecularly folded structure of (a) $\mathbf{4V}^{4(\bullet+)}$ and (b) $\mathbf{5V}^{5(\bullet+)}$. Each phenylene and $BIPY^{(\bullet+)}$ unit (green) along with adjacent single bonds (black) is counted as a free rotor.

This result presumably arises as a consequence of the drive for maximum site occupancy between the $BIPY^{(\bullet+)}$ subunits. This type of folded superstructure from the DFT for $\mathbf{3V}^{3(\bullet+)}$ is also in good agreement with the solid-state superstructure of $[\mathbf{3V}^{3(\bullet+)}]_2 \bullet 6PF_6$. On the other hand, for the intramolecular binding mode, a hairpin-like conformation is adopted, in which two terminal $BIPY^{(\bullet+)}$ subunits interact by means of radical-radical interactions within a local secondary structure, leaving the remainder of the $BIPY^{\bullet+}$ subunits unpaired and able to experience torsion around C−N single bonds. This type of folding conformation only exists when oligoviologens contain no less than four $BIPY^{(\bullet+)}$ subunits since the strain of bringing two terminal $BIPY^{(\bullet+)}$ subunits towards the desired geometry is much too large for both $\mathbf{2V}^{2(\bullet+)}$ and $\mathbf{3V}^{3(\bullet+)}$.

To estimate the entropy change of oligoviologens upon either intra- or intermolecular folding process, we assume that once two $BIPY^{(\bullet+)}$ subunits pimerize to form $[BIPY^{(\bullet+)}]_2$, the rotations of both $BIPY^{(\bullet+)}$ subunits and the corresponding xylyene linker, which includes rotations about two C–N and two C–C single bonds, are hindered. Therefore, each oligoviolgen molecule with a number of n $BIPY^{(\bullet+)}$ subunits has $4\times(n-1)$ rotors, excluding the terminal methyl group. It is noteworthy that the C–C bond between two pyridinium rings in $BIPY^{(\bullet+)}$ units does not count as

a free-rotating C–C bond, on the basis of its significant double bond character. According to this rule, for the intramolecular binding of $\mathbf{4V}^{4(\bullet+)}$ and $\mathbf{5V}^{5(\bullet+)}$, the geometry constraints reduce the number of free rotors to two $BIPY^{(\bullet+)}$ and three phenylene units, as indicated in Figure S7.

References

(1) Zhu, Z.; Li, H.; Liu, Z.; Lei, J.; Zhang, H.; Botros, Y. Y.; Stern, C. L.; Sarjeant, A. A.; Stoddart, J. F.; Colquhoun, H. M. *Angew. Chem., Int. Ed.* **2012**, *51*, 7231–7235.

(2) Fulmer, G. R.; Miller, A. J.; Sherden, N. H.; Gottlieb, H. E.; Nudelman, A.; Stoltz, B. M.; Bercaw, J. E.; Goldberg, K. I. *Organometallics* **2010**, *29*, 2176–2179.

(3) Dolomanov, O. V.; Bourhis, L. J.; Gildea, R. J.; Howard, J. A. K.; Puschmann, H. *J. Appl. Cryst.* **2009**, *42*, 339–341.